Supporting information for: Measuring Competitive Fitness in Dynamic Environments

Ivan A. Razinkov,[†] Bridget L. Baumgartner,[†] Matthew R. Bennett,[‡,¶] Lev S. Tsimring,[§,‖] and Jeff Hasty[*,†,§,⊥,#]

Department of Bioengineering, University of California San Diego, La Jolla, California, United States, Department of Biochemistry and Cell Biology, Rice University, Houston, Texas, United States, Institute of Biosciences & Bioengineering, Rice University, Houston, Texas, United States, BioCircuits Institute, University of California San Diego, La Jolla, California, United States, San diego Center for Systems Biology, La Jolla, CA 92093, USA, and San Diego Center for Systems Biology, La Jolla, CA 92093, USA

E-mail: jhasty@ucsd.edu

[*]To whom correspondence should be addressed

[†]Department of Bioengineering, University of California San Diego, La Jolla, California, United States

[‡]Department of Biochemistry and Cell Biology, Rice University, Houston, Texas, United States

[¶]Institute of Biosciences & Bioengineering, Rice University, Houston, Texas, United States

[§]BioCircuits Institute, University of California San Diego, La Jolla, California, United States

[‖]San diego Center for Systems Biology, La Jolla, CA 92093, USA

[⊥]San Diego Center for Systems Biology, La Jolla, CA 92093, USA

[#]Molecular Biology Section, Division of Biological Sciences, University of California San Diego, La Jolla, California, United States

Supporting Information

Microfluidics Device

The microfluidic device used in this study is an adapted version of the design described in Baumgartner et al.[1] The new design implemented a much larger trapping region for accommodating approximately 10^6 *S. cerevisiae* cells. To increase the viability of the device for long-term experiment (>20 days) a number of key features were added to the design. Specifically, the fluidic mixing region (DAW) was connected to the cell trap region through only a single fluidic channel. This reduced the complexity of the fluidic network during the experiments. All the fluid leaving the DAW region, exits through the sample collection port clearing all the channels between the traps of free moving cells. Effective removal of non-trapped cells is crucial for long-term viability of the device. During loading, the cells enter the device from the sample/waste collection port and flow towards the DAW region. To prevent contamination of the media ports, an auxiliary port is used to divert the flow away.

In all experiments, the cells were first grown for 24 hr in galactose-only media. Once the cells filled the trap regions, the auxiliary port (Fig. 3A, Port 5) was filled in with fast curing silicon (Sylgard 170, Dow Corning) using a 3 ml syringe, tygon tubing, and 23 gauge metal pin. After silicon curing, the cell loading syringe was removed, leaving a small piece (5-10 cm) of tubing connected to the device for sample collection into a 14 ml falcon tube. Due to the high viscosity of the uncured material, it was possible to watch silicon slowly move through the channel as slight pressure was applied on the syringe. By reducing the height and width of the auxiliary channel, thus increasing the resistance, the overflow of the silicon into the trap region was prevented. The initial sample was collected after additional 24 hr (48 hr since loading) in constant galactose-only media. Media containing glucose was labeled with a fluorescent dye, sulforhodamine 101 (0.01 mg/mL), to visualize media switching at the sample collection port. To prevent contamination reusable metal pins were autoclaved, only new sterile syringes and tubing was used for each experiment, and media were filtered through 0.22μm filters.

Since the experiments called for only bimodal switching of media, the staggered herringbone mixers (SHM) used in previous designs were not required.[1,2] Furthermore, the channel connecting the DAW region to the trap region was designed to have a gradual change in width for improved flow through the trap region.

The function of the evoDAW design was simulated with finite-element analysis software (COMSOL Multiphysics 4.0) using the Laminar Flow and Transport of Diluted Species physics simulations. Due to the large number of cells held in the device, it was important to model the glucose uptake by the cells along the entire trap. Because of the extreme length of the cell trap, there could be a point where all glucose is consumed from the medium by the cells in the trap. Downstream of that point, cells would receive medium lacking sufficient glucose levels. Our simulations show that, under the experimental conditions used, cells along the entire length of the trap receive sufficient glucose to support maximal growth rates (Figure S1-A). However, the glucose concentration at the far end of the chip (0.125% w/v) is about half that of the incoming media (0.25% w/v). Although this is a significant change, 0.125% glucose is sufficient to fully repress the galactose network.[3] Glucose consumption was calculated from glucose uptake of $r_{cell} = 5.4$ $[mmol \cdot g^{-1} \cdot hr^{-1}]$ and cell density of $\rho_{cell} = 1.130$ $[g \cdot mL^{-1}]$ to be $r_{population} = r_{cell} \cdot \rho_{cell} = 1.695$ $[mol \cdot m^{-3} \cdot s^{-1}]$.[4,5] Due to the difference in heights of the trapping region and the media channels, the volumetric consumption rate was scaled by the factor of the ratio of the channel height to trap height($\approx$16) to $0.1059[mol \cdot m^{-3} \cdot s^{-1}]$.

Fluid dynamics significantly contribute to the proper function of the evoDAW design. Uneven flow velocities could potentially create a growth advantage for individual colonies early in the experimental set up. Low flow spots could more easily accumulate a single strain of cells and form a fast growing colony that could push out neighboring colonies from the trap. To make sure our design eliminates low flow spots, we examined the velocity magnitude and streamline profiles of the entire device. The highest velocities were near the DAW region, $18[mm \cdot s^{-1}]$, while the flow velocity dropped significantly to $\approx 0.1 - 0.2[mm \cdot s^{-1}]$ in the trap region and remained constant along the entire length of the chip (Figure S1-B). This effect was due to convective deceleration; the flow

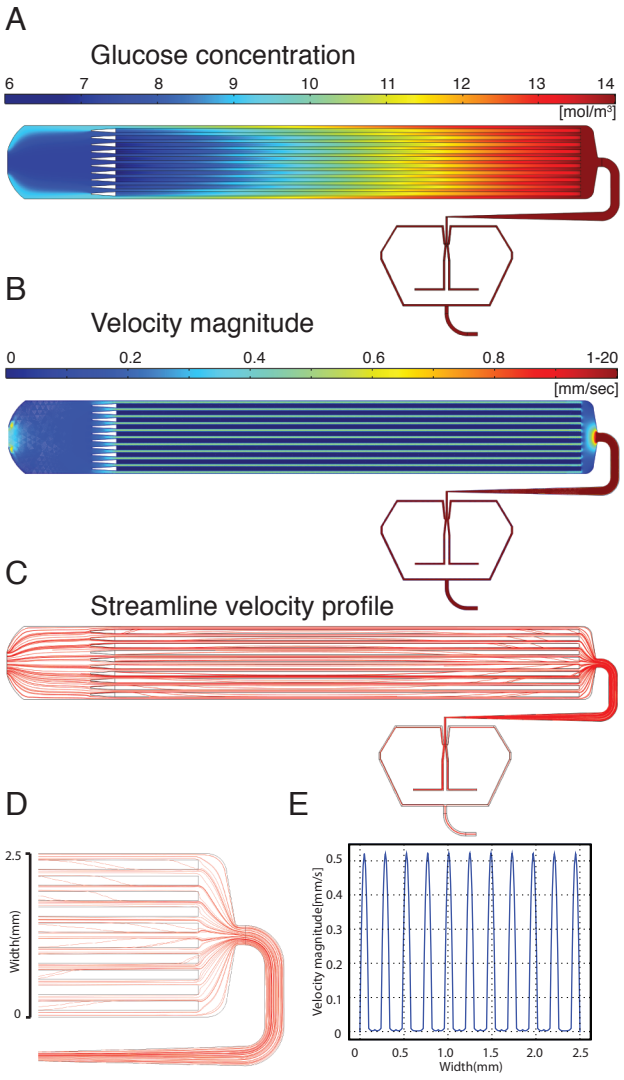

Figure S1: Finite element analysis of device design. **A**. Glucose consumption by *S. cerevisiae* was determined for the entire geometry. The initial media concentration of 0.25% w/v glucose corresponds to 14 $[mol \cdot m^{-3}]$. **B**. Velocity profile in the device. Note regarding scale: values of velocity of 1-20$[mm \cdot s^{-1}]$ are all grouped together in the same color (red). The velocity is constant in the entire trap region of the chip, exposing all the cells to similar conditions. **C**. Streamline profile of the device. Since the curvature of the streamlines is related to pressure changes perpendicular to the streamline, we can easily visualize are of large and sudden pressure changes within the device. As expected the major pressure gradients are present at the junction of trap and DAW region (**D**), while the trap region remains even. **E**. Cross-section of the trap region. Magnitude of the velocities in the traps is only a fraction of the velocity in the channels.

velocity drops when the fluid leaves a small diameter channel and enters a large one. Furthermore, it was important that all parts of the chip have the same volumetric flow rate. Simulations of the trajectories of 100 virtual beads entering the chip in the DAW region showed an even distribution of streamlines throughout the trap region (Figure S1-C and D). Lastly, it was important that cells only leave the trap due to pressure from neighboring cells and not fluid pressure. We examined the flow profiles in and around the traps. The peak velocity in the channel was 0.52 $mm \cdot s^{-1}$, while the highest velocity in the middle of the trap was $\approx$ 100 times less, 5 $\mu m \cdot s^{-1}$ (Figure S1-E).

All software and design files needed to conduct microfluidic DAW experiments are available on our wiki page: `http://dialawave.wikispaces.com`

Modeling

Section A - Derivation of Equation (2) of the main text

Assume that there are two strains, each of which grows exponentially with rate γ_{gal} while in galactose-rich media and γ_{glu} while in glucose-rich media, with $\gamma_{gal} < \gamma_{glu}$. Upon a switch from galactose to glucose at time t_s, the wild-type strain will immediately begin growing at the faster rate. If we assume constant log-phase growth, we can write the differential equation for the wild-type strain as

$$\dot{n}_{wt} = \begin{cases} \gamma_{gal} n_{wt} & t < t_s \\ \gamma_{glu} n_{wt} & t \geq t_s \end{cases} \tag{S1}$$

where n_{wt}(t) is the number of wild-type cells at time t, and the over-dot represents differentiation with respect to time. The ST strain with the randomized 5′ UTR inefficiently transitions from growth on galactose to growth on glucose. To model this, we assume that the switch between the two growth rates after the introduction of glucose is delayed by a time $\tau > 0$. Therefore, the dynamics of the randomized strain during one switch from a galactose-rich medium to a glucose-rich medium can be written as Equation (S2):

$$\dot{n}_{st} = \begin{cases} \gamma_{gal} n_{st} & t < t_s + \tau \\ \gamma_{glu} n_{st} & t \geq t_s + \tau \end{cases} \tag{S2}$$

where n_{st}(t) is the number of cells with a stabilized GAL1 transcript at time t. Solving Eqs. (S1) and (S2) gives us for time $t > t_s + \tau$

$$n_{wt}(t) = n_{wt,0} \exp\{\gamma_{gal}(t_s - t_0) + \gamma_{glu}(t - t_s)\} \tag{S3}$$

$$n_{st}(t) = n_{st,0} \exp\{\gamma_{gal}(t_s - t_0 + \tau) + \gamma_{glu}(t - t_s - \tau)\} \tag{S4}$$

where $n_{wt,0}$ and $n_{st,0}$ are the numbers of WT and ST cells at time $t_0 < t_s$, respectively.

Define the R to be the population fraction of the WT strain in a mixed population of both types of cells, i.e.

$$R \equiv \frac{n_{wt}}{n_{wt} + n_{st}} \tag{S5}$$

From Eqs. (S3) and (S4) one can show that the population fraction after one complete switch, R_1, is

$$R_1 = \frac{1}{1 + \frac{1-R_0}{R_0} \exp(-\delta\tau)} \tag{S6}$$

from which follows

$$\frac{1 - R_1}{R_1} = \frac{1 - R_0}{R_0} \exp(-\delta\tau) \tag{S7}$$

where $\delta = \gamma_{glu} - \gamma_{gal}$. Note that the population fraction only changes during the interval $(t_s, t_s + \tau)$, so that only the initial population fraction, R_0, and the final population fraction, R_1, need to be calculated. Next, assume that after one full switch from galactose to glucose, the mixed population is switched back to a galactose environment for a long enough time to return the growth rates of both strains to γ_{gal}. Because the randomized $5'$ UTR of the ST strain only affects the galactose to glucose switch, and not the reverse, there is no change in the population fraction. If the population

is then again switched to glucose for a second time, the population fraction becomes

$$R_2 = \frac{1}{1 + \frac{1-R_0}{R_0}\exp(-2\delta\tau)} \tag{S8}$$

which follows from Eq. (S7). In general, after η switches from galactose to glucose we have

$$\frac{1-R_n}{R_n} = \frac{1-R_0}{R_0}\exp(-n\delta\tau) \tag{S9}$$

giving us

$$R_n = \frac{1}{1 + \frac{1-R_0}{R_0}\exp(-n\delta\tau)} \tag{S10}$$

which is Eq. (2) of the main text.

Section B - Numerical simulation of cellular growth and division

To simulate the competitive growth of WT and ST cells, we implemented a modified version of Gillespie's algorithm. Populations of both cell types were partitioned into two groups, those in G1 phase and those in S/G2/M phases. While in G1 phase, cells spontaneously pass through START into S/G2/M, with a rate, $r_{START,i}$ that depends on both the carbon source (galactose or glucose) and the strain ($i = 1$ for WT and $i = 2$ for ST). While in galactose, this rate is given by , $r_{START,i} = r_{gal}$ for both strains. In glucose the rate is given by

$$r_{START,i} = r_{glu} - (r_{glu} - r_{gal})\exp(-\lambda_i t^*) \tag{S11}$$

where λ_i is the GAL1 mRNA degradation rate in the i^{th} strain, and t^* is the time since the last switch to glucose.

Once a cell has passed START and entered into the S/G2/M phases, it is assigned a random delay time, τ_c representing the time from the beginning of START to the completion and division

of the daughter cell. This time is given by

$$\tau_c = t_{glu/gal} + \eta \tag{S12}$$

where η is a uniformly distributed random number on $(-\sigma, \sigma)$, and $t_{glu/gal}$ is the mean delay time that depends on the current environmental carbon source. Numerically, this is achieved by removing one cell from the G1 population and adding the randomly chosen delay time into an ordered stack, representing all cells of the same strain that are currently in the S/G2/M phase. The first number in the stack then gives the time at which the next division for that strain will occur. Separate stacks are kept for each strain.

Because reactions in this simulation contain 1) reactions that do not have exponentially distributed waiting times and 2) time-dependent rates, we implemented a version of Gillespie's algorithm that incorporates both dynamical delay and time-dependent rates. First, at each incremental step a randomly chosen time step for the next reaction, τ_{exp}, is calculated from all exponentially distributed reactions, here being the spontaneous entrances into START of cells in G1 phase for both strains. Next, this randomly chosen time is compared with the time until the next delayed reaction (i.e. the minimum of all values in the two stacks), τ_{stacks}, and with a minimum step size, dt, determined by the time scales of all time-dependent rates. Here, we have $dt << 1/\lambda_i \forall i$. Depending on which of the three times above is the *least*, different outcomes occur according to Table S1.

Note that, because some of the rates in the process are time-dependent and some reactions are delayed, the entire process is non-Markovian. Setting a minimum time, in essence, does two things. First, it assumes that the entire process is locally Markovian on time scales of order dt. Second, it approximates the true continuously differentiable rate functions with piece-wise constant functions of step sizes no larger than dt.

minimum	**outcome**
τ_{exp}	The associated G1 phase cell type begins to bud. The number of G1 phase cells of that cell type is decremented by one, and a random delay time is added to the associated S/G2/M phase stack. Time is incremented by τ_{exp}.
τ_{stacks}	The exponential reaction is thrown out. The delayed reaction time is pulled from the associated stack and the number of cells in G1 phase of that cell type is incremented by two. Time is incremented by τ_{stacks}.
dt	The exponential reaction is thrown out. No reaction occurs. Time is incremented by dt.

Table S1: Modeling algorithm decision table

The total population size of the two competing strains was controlled in our stochastic simulations, as well. To do this, we implemented a chemostat-like environment that simulates constant exponential growth in a population size-limited culture. Simply, the maximum population size was set to some constant, N_{max}. Upon cellular division, i.e. exit of a cell from the S/G2/M phase, if the new population size was greater than N_{max}, a random cell, chosen from all cell types and phases, including G1 and S/G2/M phases and both cell types, was removed from the simulation. A sample single trajectory is shown in Figure S2.

The values of the constants used in our simulations are given in Table S2.

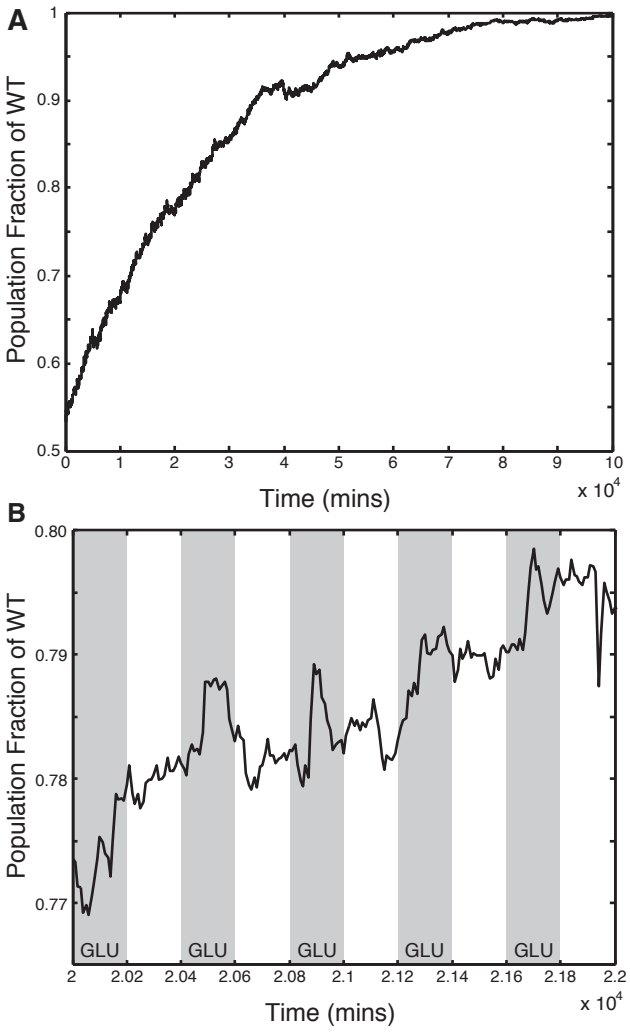

Figure S2: Numerical simulation results of a single experiment. **A**. Changes in WT population of a single stochastic simulation. Unlike the averaged data, the single simulation shows noisy behavior and sometimes sharp decreases in the WT fraction. **B**. Detailed graph showing the individual galactose-glucose switches and current WT population fraction. At this level it possible to see a stair-like change in the WT fraction corresponding to glucose switches.

Constant	Value	Units	Description
r_{glu}	ln(2)/20	min^{-1}	Rate constant for cells exiting G1 phase in the long-time limit in a glucose-rich environment.
r_{gal}	ln(2)/40	min^{-1}	Rate constant for cells exiting G1 phase in a galactose-rich environment.
λ_1	ln(2)/4	min^{-1}	Half life of GAL1 mRNA in wild-type cells in a glucose-rich envorinment.
λ_2	ln(2)/17	min^{-1}	Half life of GAL1 mRNA in mutant cells in a glucose-rich envorinment.
t_{glu}	70	min	Mean time for cells to pass through S/G2/M phases in a glucose-rich environment.
t_{gal}	80	min	Mean time for cells to pass through S/G2/M phases in a galactose-rich environment.
σ	10	min	Variance of time for cells to pass through S/G2/M phases.
N_{max}	20,000	unitless (# cells)	Maximum number of cells allowed in the simulation.
dt	0.1	min	Minimum time step.

Table S2: Simulation parameters

To test the effects of very fast switching on the population dynamics we ran the stochastic simulation with periods approaching 1 minute, Figure S3. By decreasing the period the advantage of the WT cells diminishes, requiring a larger number of switches to achieve complete take over. At a period of T=1 min, the switching happens so fast that the WT cells never take over the population, mostly likely completely filtering these fast galactose fluctuations. The deterministic model is only dependent on the number of switch and thus does not produce different results with

decreasing switching period.

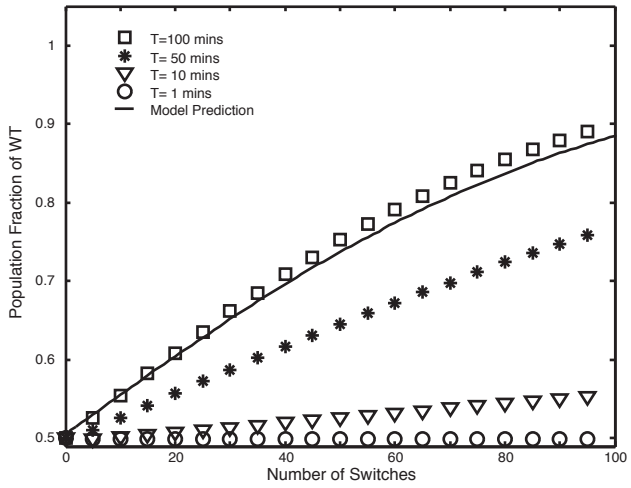

Figure S3: Numerical simulation of fast switching. Solid line shows the results of deterministic model, which is independent of the period of switching. The data points represent the results of stochastic simulations. With decreasing period the advantage of WT cell diminishes, completely disappearing at the limit of fast switching.

References

(1) Baumgartner, B. L.; Bennett, M. R.; Ferry, M.; Johnson, T. L.; Tsimring, L. S.; Hasty, J. Antagonistic Gene Transcripts Regulate Adaptation to New Growth Environments. *Proc. Natl. Acad. Sci. U. S. A.* **2011**, *108*, 21087–21092.

(2) Ferry, M. S.; Razinkov, I. A. Microfluidics for Synthetic Biology: From Design to Execution. *Methods Enzymol.* **2011**, *497*, 295–372.

(3) Bennett, M. R.; Pang, W. L.; Ostroff, N. A.; Baumgartner, B. L.; Nayak, S.; Tsimring, L. S.; Hasty, J. Metabolic Gene Regulation in a Dynamically Changing Environment. *Nature* **2008**, *454*, 1119–1122.

(4) van Dijken, J. P.; Weusthuis, R. A.; Pronk, J. T. Kinetics of Growth and Sugar Consumption in Yeasts. *Antonie van Leeuwenhoek* **1993**, *63*, 343–352.

(5) Bryan, A. K.; Goranov, A.; Amon, A.; Manalis, S. R. Measurements of Mass, Density, and Volume During the Cell Cycle of Yeast. *Proc. Natl. Acad. Sci. U. S. A.* **2010**, *107*, 999–1004.